Accepted Manuscript

Computers & Fluids, Volume 38, Issue 6, June 2009, Pages 1232-1242

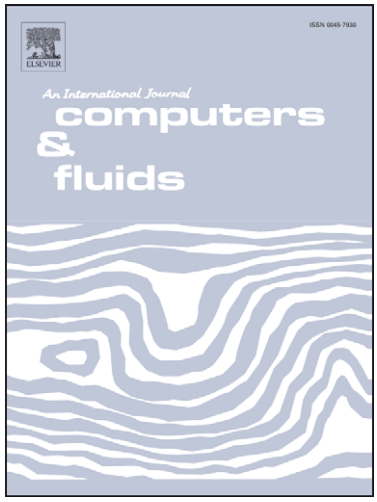

Study of Jet Precession, Recirculation and Vortex Breakdown in Turbulent Swirling Jets Using LES

K.K.J. Ranga Dinesh, M.P. Kirkpatrick

PII: S0045-7930(08)00231-4
DOI: 10.1016/j.compfluid.2008.11.015
Reference: CAF 1114

To appear in: *Computers & Fluids*

Received Date: 10 July 2008
Revised Date: 24 November 2008
Accepted Date: 25 November 2008

Please cite this article as: Dinesh, K.K.J.R., Kirkpatrick, M.P., Study of Jet Precession, Recirculation and Vortex Breakdown in Turbulent Swirling Jets Using LES, *Computers & Fluids* (2008), doi: 10.1016/j.compfluid.2008.11.015

Study of Jet Precession, Recirculation and Vortex Breakdown in Turbulent Swirling Jets Using LES

K.K.J.Ranga Dinesh [1], M.P.Kirkpatrick [2]

1. School of Engineering, Cranfield University, Cranfield, Bedford, MK43 0AL, UK.
2. School of Aerospace, Mechanical and Mechatronic Engineering, The University of Sydney, NSW 2006, Australia.

Corresponding author: K.K.J.Ranga Dinesh

Email address: Ranga.Dinesh@Cranfield.ac.uk

Postal Address: School of Engineering, Cranfield University, Cranfield, Bedford, MK43 0AL, UK.

Telephone number: +44 (0) 1234750111 ext 5350

Fax number: +44 1234750195

Revised Manuscript prepared for the Journal of Computers and Fluids

24th November 2008

Study of Jet Precession, Recirculation and Vortex Breakdown in Turbulent Swirling Jets Using LES

K.K.J.Ranga Dinesh [1], M.P.Kirkpatrick [2]

ABSTRACT

Large eddy simulations (LES) are used to investigate turbulent isothermal swirling flows with a strong emphasis on vortex breakdown, recirculation and instability behavior. The Sydney swirl burner configuration is used for all simulated test cases from low to high swirl and Reynolds numbers. The governing equations for continuity and momentum are solved on a structured Cartesian grid, and a Smagorinsky eddy viscosity model with the localised dynamic procedure is used as the subgrid scale turbulence model. The LES successfully predicts both the upstream first recirculation zone generated by the bluff body and the downstream vortex breakdown bubble. The frequency spectrum indicates the presence of low frequency oscillations and the existence of a central jet precession as observed in experiments. The LES calculations well captured the distinct precession frequencies. The results also highlight the precession mode of instability in the centre jet and the oscillations of the central jet precession, which forms a precessing vortex core. The study further highlights the predictive capabilities of LES on unsteady oscillations of turbulent swirling flow fields and provides a good framework for complex instability investigations.

Key words: Swirl, Recirculation, Vortex breakdown, Precessing vortex core, Strouhal number, Large eddy simulation

I. INTRODUCTION

Swirling flows are frequently found in nature and also occur in a wide range of practical applications, such as gas turbine combustors, agricultural spraying machines, whirlpools, cyclone separators and vortex shedding from aircraft wings. Since the majority of swirling flows operate in a turbulent environment, it is necessary to consider the unsteady flow oscillations during the flow evolution. Investigation of precession, recirculation, vortex breakdown and instabilities have received much attention [1-5] and recently several groups have studied the jet precession, oscillation mechanisms and the role of precessing vortex core (PVC) in which the centre of the vortex precesses around the central axis of symmetry [6-7]. In combustion systems, these phenomena promote the coupling between combustion, flow dynamics and acoustics [7].

Several groups have identified various forms of precession motion and instability modes in both reactive and non-reactive swirling flow fields [8-9]. Experimental evidence has shown that, configurations, the existence of a PVC depends on the occurrence of vortex breakdown and on having a swirl number greater than its critical value [10]. However, PVC also occurs at low values of swirl number where a swirling jet is released into a large expansion. Dellenback et al. [11] observed several precession mechanisms in experiments involving swirling pipe flow over a range of high swirl numbers. Alternatively, Sozou and Switenbank [12] carried out an analytical calculation using an inviscid model for PVC phenomena and found a reasonable agreement with the data of Chanaud [10] and Cassidy et al. [13]. Averamenko et al. [14] carried out further investigations and found that the PVC frequency is linearly dependent on both the mean inlet velocity and is a weak function

of viscosity. Sato et.al. [15] carried out the first computational modelling work using the Reynolds averaged Navier-Stokes (RANS) technique for the PVC phenomena and deduced a number of oscillation mechanisms. Guo et al. [16] carried out a RANS simulation for a turbulent swirl flow passing into a sudden expansion, and found a large PVC structure and a particular combination of precession and flapping oscillations for zero swirl strength. However, RANS based methods are only successful for flows with non-gradient transport and therefore do not provide the level of accuracy required for the prediction of a large scale highly unsteady PVC.

Large eddy simulation (LES) has been widely accepted as a promising numerical tool for solving the large-scale unsteady behavior of complex turbulent flows. Encouraging results have been reported in recent literature and demonstrate the ability of LES to capture the swirling flow instability and the energy containing coherent motion of the PVC. For example, Wegner et al. [17] carried out LES calculations for isothermal swirling flow fields and captured the PVC phenomena with a good degree of success. Roux et al. [18] performed an LES of an isothermal flow field in a gas turbine combustor and accurately predicted both the major PVC oscillation frequency and a strong second acoustic mode. This example, further demonstrates the capability of LES to capture the strong coupling between the acoustics and the swirling flow dynamics. Selle et al. [19] also carried out LES of an industrial gas turbine burner and captured the entire PVC structure of the isothermal flow field. Wang et al. [20] detected the low frequency oscillations and precession for their LES calculations of confined isothermal swirl flows. Recently, Wang et al. [21] conducted LES calculations of flow dynamics for an operational aero engine combustor and found encouraging results for the PVC phenomena.

Despite extensive reviews, the investigation of unsteady flow oscillations such as vortex shedding and the occurrence of the PVC in swirl stabilized systems remains a challenge. Interactions between different instability modes can cause considerable noise fluctuations as a result of the oscillating pressure field. Further investigations are necessary to identify the link between the oscillation mechanisms and the jet precession in swirl stabilized jets [4][9].

The present work focuses on a series of LES calculations for isothermal flow fields based on the Sydney swirl burner configuration and demonstrates the features of jet precession (often starting at moderate swirl number) as well as the existence of PVC associated with a bluff body [22-24]. The Sydney swirl burner configuration has also been extensively investigated as a target model problem for computations in the Proceedings of Turbulent Non-Premixed Flames (TNF) group meetings [25].

The swirl configuration used in this work features unconfined swirling flow fields generated by an upstream recirculation zone and a second downstream recirculation zone induced by swirl, which greatly improves the mixing process. In addition, the swirling flow fields generate central jet precession and a PVC structure close to the burner exit. The ultimate goal of this paper is to present the correlations between axial, swirl and vortex breakdown instabilities associated with central jet precession and analysis the occurrence of PVC using the Strouhal number and geometric swirl number.

In our earlier studies, we have shown that LES accurately predicts different isothermal swirling flow fields of the Sydney swirl flame series [26], and later have extended the work to reacting cases [27-28]. The current work is a continuation of our investigations of flow recirculation, vortex breakdown, oscillations and instabilities associated with the isothermal swirling flow fields. Results will be presented for the power spectra, Strouhal and swirl numbers.

The layout of this paper is as follows. Section II presents the details of Sydney swirl burner configuration. In Section III we will present the computational method including the governing equations, discretisation methods and boundary conditions. Results from the simulations and comparison with experimental data will be discussed in Section IV. Finally, a short summary in Section V will conclude the main findings of this paper.

II. THE SYDNEY SWIRL BURNER

A schematic of the Sydney swirl burner configuration used in this work is shown in Fig. 1. It has a 60mm diameter annulus for a primary swirling air stream surrounding the circular bluff body of diameter D=50mm with a 3.6mm diameter central fuel jet. The jet fluid for isothermal cases is air. The burner is housed in a secondary co-flow wind tunnel with a square cross section of 130mm sides. Swirl is introduced aerodynamically into the primary annulus air stream 300mm upstream of the burner exit plane and inclined 15 degrees upward to the horizontal plane. The swirl number can be varied by changing the relative magnitude of tangential and axial flow rates. Velocity measurements were made at the University of Sydney [22-24]. The literature already includes the details flow conditions such as flow types, their velocities, swirl

and Reynolds numbers [23-24]. The flow conditions considered in the simulations presented here are shown in Table 1. Here U_j is the central jet velocity, U_s is the bulk axial velocity of the annulus, Sg is the swirl number, Re_j and Re_s are the Reynolds numbers of the jet and annulus respectively.

U_j	$U_s = 16.3$ $\mathrm{Re}_s = 32{,}400$	$U_s = 29.7$ $\mathrm{Re}_s = 59{,}000$	Re_j
66	S_g 0.57-0.91	S_g 0.28-0.45	14300

Table 1.The flow conditions considered for simulations [24]

III. COMPUTATIONAL METHOD

A. Mathematical formulations and numerical methods

In LES the large energy containing scales of motion are resolved numerically while the effect of the small, unresolved scales is modeled. The flow is assumed to be isothermal and incompressible. Applying a spatial box filter to Navier-Stokes equations, we obtain the filtered continuity and momentum equations for the large-scale motion as follows

$$\frac{\partial \overline{u}_j}{\partial x_j} = 0 \tag{1}$$

$$\frac{\partial \overline{u}_i}{\partial t} + \frac{\partial (\overline{u}_i \overline{u}_j)}{\partial x_j} = -\frac{1}{\rho}\frac{\partial \overline{P}}{\partial x_i} + \frac{\partial (2\nu \overline{S}_{ij})}{\partial x_j} - \frac{\partial (\tau_{ij})}{\partial x_j}. \tag{2}$$

Here u_i, p, ρ, ν denote the velocity, pressure, density, kinematic viscosity and the strain rate tensor $S_{ij} = \frac{1}{2}\left(\frac{\partial \overline{u}_i}{\partial x_j} + \frac{\partial \overline{u}_j}{\partial x_i}\right)$.

The last term in equation (2) is the divergence of the SGS stress tensor, which represents the sub-grid scale (SGS) contribution to the momentum. Hence, subsequent modelling is required for $\tau_{ij} = \left(\overline{u_i u_j} - \overline{u}_i \overline{u}_j\right)$ to close the system of equations. The Smagorinsky eddy viscosity model [29] is used here to model the SGS stress tensor as

$$\tau_{ij} - \frac{1}{3}\delta_{ij}\tau_{kk} = -2\nu_{sgs}\overline{S}_{ij}\,. \tag{3}$$

Here the eddy viscosity ν_{sgs} is a function of the filter size and strain rate

$$\nu_{sgs} = C_s \overline{\Delta}^2 \left|\overline{S}\right|, \tag{4}$$

Where C_s is a Smagorinsky model parameter [29], $\overline{\Delta}$ is the filter width and $|\overline{S}| = (2\overline{S}_{ij}\overline{S}_{ij})^{\frac{1}{2}}$. The localized dynamic procedure of Piomelli and Liu [30] was used to obtained the model parameter C_s, which appears in equation (4) as a part of the SGS turbulence modelling. This model uses information in the resolved flow fields to determine the model parameter dynamically. As such, the parameter varies in both time and space based on local flow conditions.

The governing equations are discretised on a non-uniform, three dimensional, staggered Cartesian grid by using the LES code PUFFIN originally developed by Kirkpatrick [31] and later extended by Ranga Dinesh. [32]. PUFFIN calculates the temporal development of large-scale flow structures by solving the filtered LES equations for mass and momentum (Eq. 1 and 2). The LES equations are discretised in space using a finite volume method. A second order central difference scheme is used for the spatial discretisation of momentum equations and pressure correction equation. First, the momentum equations are integrated using a third order hybrid Adam-Bashforth/ Adam-Moulton scheme to give an approximate solution for the

velocity field. Mass conservation is enforced through a pressure correction step in which the approximate velocity field is projected onto a subspace of divergence free velocity fields. The pressure correction method of Van Kan [33] and Bell et al. [34] was used in the present calculations. The solution is advanced with a time step corresponding to Courant number less than 0.6. The equations, discretised as described above, are solved using a linear equation solver. Here a Bi-Conjugate Gradient Stabilized (BiCGStab) solver with a Modified Strongly Implicit (MSI) preconditioner is used. The momentum residual error is typically of the order 10^{-5} per time step and the mass conservation error is of the order of 10^{-8}. Further details of the numerical methods used can be found in Kirkpatrick et al. [35-37]

C. Boundary conditions

This section describes the boundary conditions used for the simulations. The mean velocity distributions for the jet and annulus flows were specified using power law velocity profiles [26-28]. The mean profiles for both axial and swirl velocities are specified by a power law of the form

$$< U >= 1.218 U_j \left(1 - \frac{|y|}{\delta}\right)^{1/7}, \qquad (5)$$

Where U_j is the bulk velocity, y the radial distance from the jet centre line and $\delta = 1.01 R_j$, where R_j is the fuel jet radius of 1.8 mm. The factor 1.01 is added to ensure that velocity gradients are finite at the walls. The same equation is used for the swirling air stream with U_j replaced by the bulk axial velocity U_s and bulk tangential velocity W_s, y the radial distance from the centre of the annulus and $\delta = 1.01 h/2$, where h is the width of the annulus. Turbulence at the inlets is modelled by superimposing fluctuations on the mean velocity profiles generated from a

Gaussian distribution such that the inflow has the correct turbulence kinetic energy levels obtained in the experimental data. At solid walls a free slip condition is applied. At the outlet, a convection boundary condition is used.

D. Domain size, grid and statistics

The computations were performed on non-uniform Cartesian grid in a domain with dimensions $300\times300\times250mm$. The grid has $100\times100\times100$ cells in the x, y and z directions respectively giving a total of one million cells. Grid lines in the x and y directions use an expansion ratio of $\gamma_{xy}=\Delta x(i)/\Delta x(i-1)=1.08$ and an expansion ratio of $\gamma_z=1.07$ is used in the z-direction. A grid sensitivity analysis for a high swirl case (swirl number 1.59) published in our earlier work [26] indicated that reasonable grid independence is achieved for the mean velocity fields and Reynolds stresses with this grid. All simulations were carried out for the total time period of $300ms$ and two non-consecutive sampling periods yielded similar results indicating that the statistics were well converged.

IV. RESULTS AND DISCUSSION

The Sydney swirl burner is designed to study reacting and non-reacting swirling flows for a range of swirl numbers and Reynolds numbers. This section discusses the LES results focussing on features of the swirling flow fields such as recirculation, vortex breakdown, central jet oscillation and PVC structures for various flow conditions. First the occurrence of vortex breakdown, recirculation and its relationship with the swirl number will be discussed. Results will then be presented to demonstrate the central jet precession and PVC structures for different flow conditions. Finally, a comparison plot for a Strouhal number will be discussed. The results obtained from

the LES calculations will be discussed in two cases. Case I involves flow features for moderate swirl numbers at the primary annulus axial velocity of $U_s = 29.7$ m/s, while Case II involves high swirl numbers at the primary annulus axial velocity of $U_s = 16.3$ m/s.

Case I: Analysis of recirculation, vortex breakdown, precession frequencies, precessing vortex core (PVC) and Strouhal number for $U_s = 29.7$ m/s at swirl numbers $S_g = 0.28, 0.34, 0.40, 0.45$.

A. Recirculation and vortex breakdown

Fig. 2 shows four contour plots of mean axial velocity and clearly shows the upstream recirculation zone and downstream vortex breakdown. For swirl numbers 0.28, 0.34, no negative velocities are observed on the centreline and hence no vortex bubble formed. For swirl numbers, 0.40, 0.45, the mean axial velocity becomes negative on the centreline, which indicates the occurrence of a vortex breakdown bubble (VBB). Increasing the swirl number also increases the axial extent of the vortex bubble. Figs. 3 and 4 show isosurfaces of the negative mean axial velocity at a value of -0.2 m/s for swirl numbers 0.40 and 0.45 respectively. The plots reveal that the expansion of the upstream recirculation zone is similar; however the growth of the downstream vortex bubble differs slightly. We have also found that the increased swirl velocity has a minor impact on the formation of VBB in the downstream region and that the VBB promotes the shear layer instability in the downstream recirculation zone.

Fig. 5 shows the calculated centerline mean axial velocity for a range of swirl numbers $S_g = 0.28,0.34,0.40,0.45$. The calculations of centerline negative mean axial velocity indicates a flow reversal. For the cases with swirl numbers 0.40 and 0.45, the greatest negative axial velocities of -2.7 m/s and -4.5 m/s occur at approximately x=80mm and x=65mm respectively. For these two cases, the mean axial velocity is negative within the range of x=70 – 95mm and x=47 – 90mm respectively. The jet velocity decays in a similar manner in the downstream section for all cases.

B. Precession frequencies and precessing vortex core (PVC)

Figs. 6-8 show the power spectra for swirl numbers 0.34, 0.40 and 0.45 at the spatial jet locator. The spatial jet locator is positioned just off the burner centerline at x=12.3mm (axial location) and r=2.3mm (radial location) similar to the experimental investigation. A pair of monitoring points are used on either side of the centre jet [22-24]**.**

The power spectrum is constructed by applying the Fast Fourier Transform (FFT) to the instantaneous axial velocity at the jet locator point. The power spectrum for the case $S_g = 0.34$ has a distinct peak at a frequency of ~24 Hz, which indicates the occurrence of precession. The power spectrum for $S_g = 0.40$ has a number of peaks at low frequency with the highest at approximately 24Hz, which is slightly lower to than that found in the experimental observation (26Hz) [24]. The spectrum for $S_g = 0.40$ also has smaller peaks at 50Hz and 75Hz. These may be attributed to the critical swirl number for downstream VBB, where the VBB start to disappear. The power spectrum for $S_g = 0.45$ has the highest peak at ~26Hz. All distinct precession

frequencies obtained from the present simulations are very close to the experimentally observed values [24].

Figs. 9 and 10 show instantaneous isosurfaces of static pressure at $S_g = 0.40,0.45$ and demonstrate the PVC structure outlined by a pressure value of *p*= -85Pa. In the low swirl case ($S_g = 0.40$) the PVC structure is more coherent than in the high swirl case ($S_g = 0.45$) and both PVC structures occur at same central jet precession frequency value. For both cases, the low-pressure core aligns with the centerline. The upstream extent of the vortex bubble is much larger for the case $S_g = 0.45$ than for 0.40, which changes the downstream PVC structure as shown in Fig. 10.

C. Strouhal number

The Strouhal number plays a vital role in detecting precession motion and provides a basis for precession analysis in both isothermal and reacting swirl flow applications. Conventionally, the Strouhal number can be defined as fDe^3/Q, where f is the frequency, De is the exhaust diameter of the swirl burner and Q is the volumetric flow rate [9]. For this study, the Strouhal number is calculated as $St = 2fr_s/W_s$, which is consistent with the experimental definition [24]. Here again, f is a precession frequency, r_s is the radius of the bluff body and W_s is the tangential velocity of the primary annulus. Fig. 11 shows good agreement between predicted and measured values of Strouhal number for detected precession frequencies. The only discrepancy appears for the case $S_g = 0.40$ for which the LES underestimates the precession frequency.

Case II: Analysis of recirculation, vortex breakdown, precession frequencies, precessing vortex core (PVC) and Strouhal number for $U_s = 16.3$ m/s at swirl numbers $S_g = 0.57, 0.68, 0.91$.

A. Recirculation and vortex breakdown

Fig. 12 contains contour plots of the mean axial velocity showing the upstream recirculation zone and the downstream VBB at the three swirl numbers. The downstream vortex bubble is only formed for swirl numbers 0.57 and 0.68. Despite having the highest swirl number, no vortex bubble is formed for the case $S_g = 0.91$. Therefore the downstream flow reversal disappears at some intermediate swirl number between $S_g = 0.68$ and 0.91. Similar behaviour has been observed by the experimental investigation [24]. Fig. 13 shows the predicted centerline mean axial velocity for the three test cases. A small vortex bubble is formed only for the swirl number $S_g = 0.57, 0.68$. The stagnation point occurs at $x = 70mm$ for $S_g = 0.57$ and at $x = 82mm$ for $S_g = 0.68$. The jet velocity decays in a similar manner in the upstream section and varies slightly in the range $x = 40 - 100mm$ as a result of the downstream recirculation zone. In case II, the flow conditions are different and hence size of the downstream VBB is significantly smaller than that found in case I.

B. Precession frequencies and precessing vortex core (PVC)

The power spectra at a spatial jet locator are shown in Figs. 14-16. Fig. 14 shows the power spectrum for a case $S_g = 0.57$. The LES calculates a precession frequency value of 30Hz, which is slightly greater than the experimental value (28Hz) [24]. The

power spectrum for $S_g = 0.68$ accurately predicts the precession frequency value of 28Hz in comparison to the experimental value (see Fig. 15).

As shown in Fig. 16, for $S_g = 0.91$ the LES gives a precession frequency value of 26Hz and contains high peaks in the low frequency range. The cases $S_g = 0.68$ and 0.91 have more distinct peaks at the precession frequency than $S_g = 0.57$ and the calculated precession frequency values are much closer to the experimental values [24]. Fig. 17-19 show instantaneous isosurfaces of static pressure for swirl numbers $S_g = 0.57, 0.68, 0.91$ respectively. As with the PVC for the lower swirl numbers shown in Figs. 9 and 10, it can be seen that the complexity of the PVC increases as the swirl number increases.

C. Strouhal number

Fig. 20 shows the agreement between the predicted and measured values of Strouhal number based onthe precession frequency. The only discrepancy with the experimental value appears at $S_g = 0.57$ where the LES slightly overestimates the precession frequency. This further demonstrates the possibility of using LES to study the jet precession and oscillation mechanisms in turbulent swirling flows.

V. CONCLUSIONS

In this paper we have reported results for large eddy simulations of isothermal swirling flows based on the Sydney swirl burner, which was experimentally investigated by Al-Abdeli and Masri [23-25]. Two major test cases based on different primary annulus axial velocity have been considered. The two major cases were

further divided into seven different test cases based on different swirl numbers in order to study the influence of swirl number on recirculation, vortex breakdown, precessing vortex core and precession frequencies.

The LES successfully simulated the recirculation zones, vortex breakdown bubbles and precessing vortex cores for all test cases. In particular, the precession frequencies for the central jet precession have been captured and are in excellent agreement with the experimental measurements as seen through a comparison of the Strouhal numbers [24]. There appears to be a relation between the central jet precessions and the axial extent of the vortex bubble, however, further investigation is required to explore the relationship between the central jet precession and the downstream vortex bubble. The results of this study show that LES seems to be suitable for investigating instabilities in swirling jets. This is an important finding, since there is a need for more fundamental LES investigations on the mechanisms of instability modes and PVC in combustion systems. Further work on coupling mechanisims between instability and combustion would certainly help to improve the knowledge of combustion instabilities in swirl combustion systems and we intend to extend our work for the instability analysis of swirl combustion systems.

REFERENCES

[1] Sarpkaya T. On stationary and traveling vortex breakdowns. J. Fluid Mech 1971; 45: 545-559

[2] Escudier M, Zehinder N. Vortex-flow regimes. J. Fluid Mech 1982; 115: 105-121

[3] Escudier M. Vortex breakdown: observations and explanations. Prog. Aero. Sci 1988; 25: 189-229

[4] Lucca-Negro O, O'Doherty TO. Vortex breakdown: a review. Prog. Ener. Comb. Sci 2001; 27: 431-481

[5] Gupta AK, Lilley DJ, Syred N. Swirl flows. Tunbridge Wells, UK: Abacus Press 1984

[6] Froud D, O'Doherty T, Syred N. Phase averaging of the precessing vortex core in a swirl burner under piloted and premixed combustion conditions. Combust. Flame 1995; 100: 407-417

[7] Syred N, Fick W, O'Doherty T, Griffiths AJ. The effect of the precessing vortex core on combustion in swirl burner. Combust. Sci. Tech 1997; 125: 139-157

[8] Syred N, Beer JM. Combustion in swirling flows: a review. Combust. Flame 1974; 23: 143-201

[9] Syred N. A review of oscillation mechanisms and the role of the precessing vortex core (PVC) in swirl combustion systems. Prog. Energy. Combust. Sci 2006; 32: 93-161

[10] Chanaud RC. Observations of oscillatory motion in certain swirling flows. J. Fluid. Mech 1965; 21(1): 111-121

[11] Dellenback PA, Metzger D, Neitzel G. Measurements in turbulent swirling flow through an abrupt axisymmetric expansion. AIAA Journal 1998; 26(6): 669-680

[12] Sozou C, Swithenbank J. Adiabatic transverse waves in a rotation fluid. J. Fluid. Mech 1963; 38(4): 657-671

[13] Cassidy J, Falvey H. Observations of unsteady flow arising after vortex breakdown. J. Fluid Mech 1965; 21(1): 11-22

[14] Averamenko A, Bowen P, Kobzar S, Syred N, Khalatov A, Griffiths A. Analytical analysis of three dimensional instabilities existing in industrial swirl generators. ASME Fluid Eng. Div. summer meeting 1997; June 22-26

[15] Sato K, O'Doherty T, Biffin M, Syred N. Analysis of strong swirling flows in a swirl burner/furnaces. Proceedings of the international symposium on combustion and emission control, Institute of Energy 1993; 243-247

[16] Guo B, Langrish T, Fletcher D. CFD simulation of precession in sudden pipe expansion flows with inlet swirl. Applied Mathe. Model 2002; 26: 1-10

[17] Wenger B, Maltsev A, Schneider C, Sadiki A, Dreizler A, Janicka J. Assessment of unsteady RANS in predicting swirl flow instability based on LES and experiments. Int. J. Heat Fluid Flow 2004; 25: 28-36

[18] Roux S, Lartigue G, Poinsot T, Meier U, Berat C. Studies of mean and unsteady flow in s a swirled combustor using experiments, acoustic analysis and large eddy simulations. Combust. Flame 2005; 141: 40-54

[19] Selle L, Lartigue G, Poinsot T, Koch R, Schildmacher K, Krebs W, et al. Compressible large eddy simulation of turbulent combustion in complex geometry on unstructured meshes. Combust. Flame 2004; 137: 489-505

[20] Wang P, Bai X, Wessman M, Klingmann J. Large eddy simulation and experimental studies of a confined turbulent swirling flow. Phy. Fluids 2004; 16: 3306-3324

[21] Wang S, Yang V, Hsiao G, Hsieh S, Mongia H. Large eddy simulations of gas turbine swirl injector flow dynamics. J. Fluid. Mech 2007; 583: 99-122

[22] Al-Abdeli Y. Experiments in Turbulent swirling non-premixed flame and isothermal flows. PhD Thesis, School of Aero. Mech. Mecha. Eng., University of Sydney, Australia 2003

[23] Al-Abdeli Y, Masri AR. Recirculation and flow field regimes of unconfined non-reacting swirling flow. Exp. Therm. Fluid Sci 2003; 23: 655-665

[24] Al-Abdeli Y, Masri AR. Precession and recirculation in turbulent swirling isothermal jets. Combust. Sci. Tech 2004; 176: 645-665

[25] Barlow RS. Turbulent non-premixed swirling flames. Proceedings of the 8th International workshop on Turbulent Non-premixed Flames 2006; Germany

[26] Malalasekera W, Ranga Dinesh KKJ, Ibrahim SS, Kirkpatrick MP. Large eddy simulation of isothermal turbulent swirling jets. Combust. Sci. Tech 2007; 179: 1481-1525

[27] Malalsekera W, Ranga Dinesh KKJ, Ibrahim SS, Masri AR. LES of recirculation and vortex breakdown in swirling flames. Combust. Sci. Tech 2008; 180: 809-832

[28] Kempf, A, Malalasekera, W, Ranga Dinesh KKJ, Stein O. Large eddy simulation with swirling non-premixed flames with flamelet model: A comparison of numerical methods. Flow Turb. Combust 2008; Online first

[29] Smagorinsky, J. General circulation experiments with the primitive equations. M. Weather Review. 1963; 91: 99-164

[30] Piomelli, U. and Liu, J. Large eddy simulation of channel flows using a localized dynamic model. Phy. Fluids 1995; 7: 839-848.

[31] Kirkpatrick MP. Large eddy simulation code for industrial and environmental flows. PhD Thesis, University of Sydney, Australia. 2002

[32] Ranga Dinesh KKJ. Large eddy simulation of turbulent swirling flames. PhD Thesis, Loughborough University, UK. 2007

[33] Van Kan J. Second order accurate pressure correction scheme for viscous incompressible flow. SIAM J Sci. Stat Comput 1986; 7: 870-891

[34] Bell J, Colella P, Glaz H. A second order projection method for the incompressible Navier-Stokes equations. J. Comp. Phys 1989; 85: 257-283

[35] Kirkpatrick MP, Armfield SW, Kent JH. A representation of curved boundaries for the solutions of the Navier-Stokes equations on a staggered three dimensional Cartesian grid. J. Comput. Phy 2003; 104: 1-36

[36] Kirpatrick MP, Armfield SW, Kent JH, Dixon TF. Simulation of vortex shedding flows using high-order fractional step methods. ANZIAM J 2000; 43 (e): 856-876

[37] Kirkpatrick, MP, Armfield. On the stability and performance of the projection-3 method for the time integration of the Navier-Stokes equations. ANIZIAM J 2008; 49:559-575

FIGURE CAPTIONS

Fig. 1: Schematic drawing of the Sydney swirl burner

Fig. 2: Contour plots of mean axial velocities (in m/s) at $U_s = 29.7$ m/s

Fig. 3: Isosurface of negative mean axial velocity (-0.2 m/s) for swirl number 0.40

Fig. 4: Isosurface of negative mean axial velocity (-0.2 m/s) for swirl number 0.45

Fig. 5: Mean centerline axial velocity for range of swirl numbers at $U_s = 29.7$ m/s

Fig. 6: Power spectrum (W/Hz) at spatial jet locator for swirl number 0.34

Fig. 7: Power spectrum (W/Hz) at spatial jet locator for swirl number 0.40

Fig. 8: Power spectrum (W/Hz) at spatial jet locator for swirl number 0.45

Fig. 9: Precessing vortex core visualised by isocontours of pressure for swirl number 0.40

Fig. 10: Precessing vortex core visualised by isocontours of pressure for swirl number 0.45

Fig. 11: Variation of Strouhal number with swirl number. Diamonds represent LES results and square symbol represent experimental measurements

Fig.12: Contour plots of mean axial velocities (in m/s) at $U_s = 16.3$ m/s

Fig. 13: Mean centerline axial velocity for range of swirl numbers at $U_s = 16.3$ m/s

Fig. 14: Power spectrum (W/Hz) at spatial jet locator for swirl number 0.57

Fig. 15: Power spectrum (W/Hz) at spatial jet locator for swirl number 0.68

Fig. 16: Power spectrum (W/Hz) at spatial jet locator for swirl number 0.91

Fig. 17: Precessing vortex core visualised by isocontours of pressure for swirl number 0.57

Fig. 18: Precessing vortex core visualised by isocontours of pressure for swirl number 0.68

Fig. 19: Precessing vortex core visualised by isocontours of pressure for swirl number 0.91

Fig. 20: Variation of Strouhal number with swirl number. Diamonds represent LES results and square symbol represent experimental measurements

FIGURES

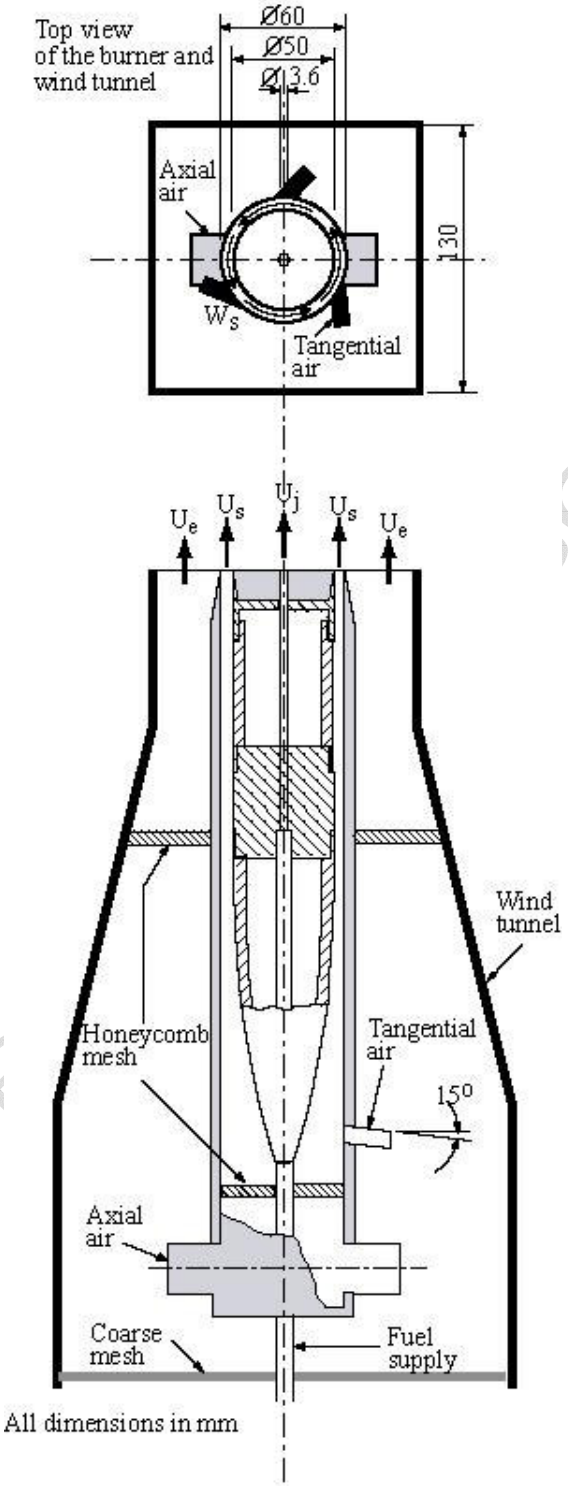

Fig. 1. Schematic drawing of the Sydney swirl burner

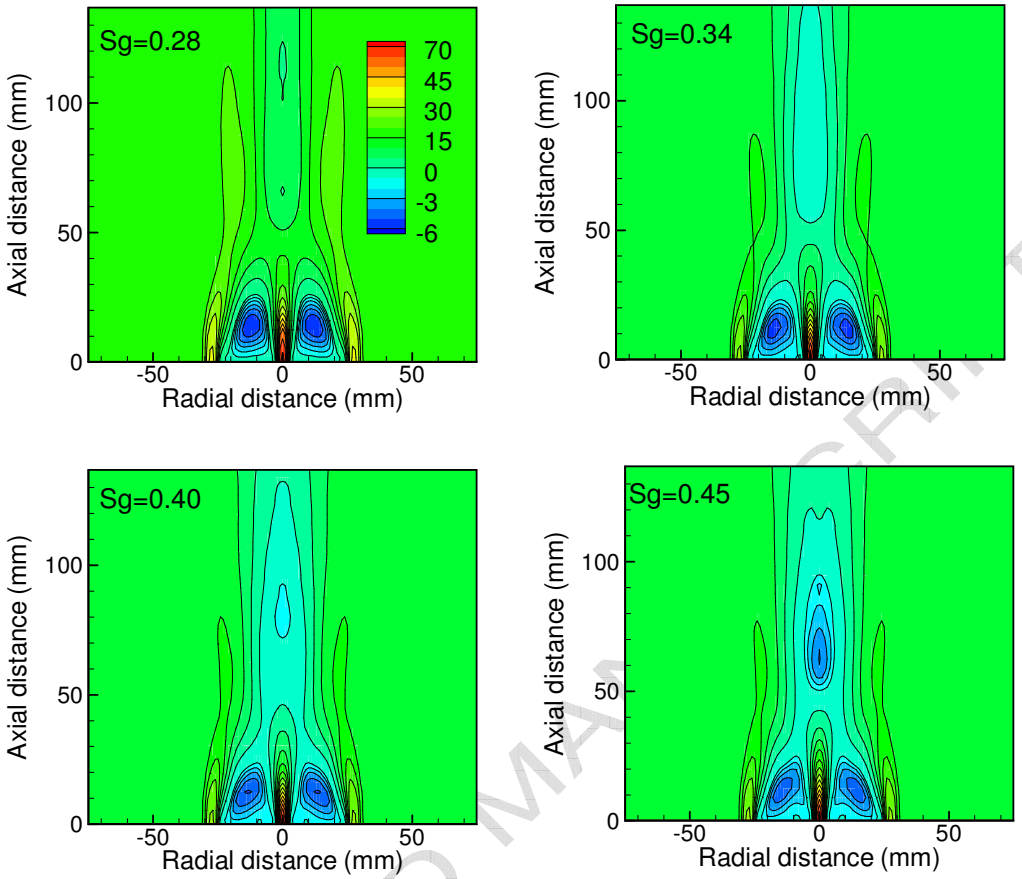

Fig. 2. Contour plots of mean axial velocities (in m/s) at $U_s = 29.7$ m/s

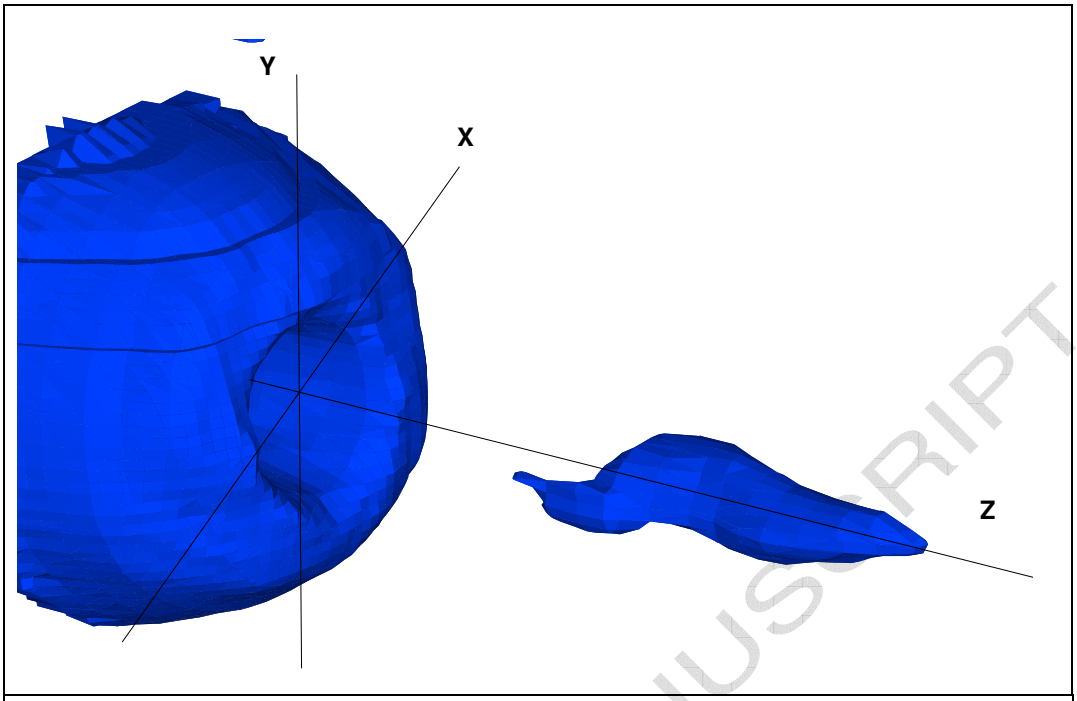

Fig 3. Isosurface of negative mean axial velocity (-0.2 m/s) for swirl number 0.40

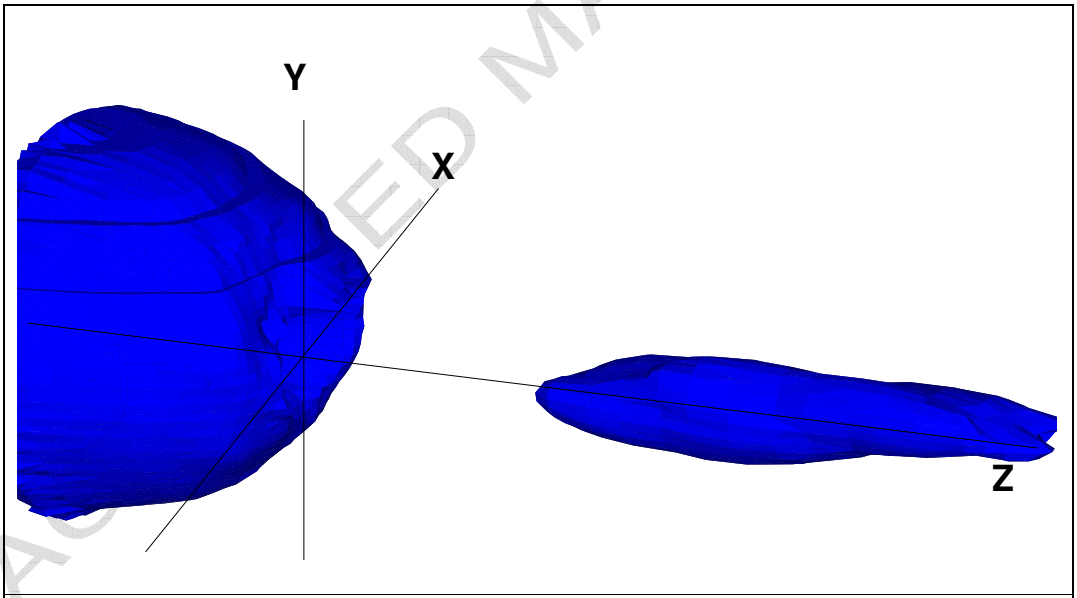

Fig. 4. Isosurface of negative mean axial velocity (-0.2 m/s) for swirl number 0.45

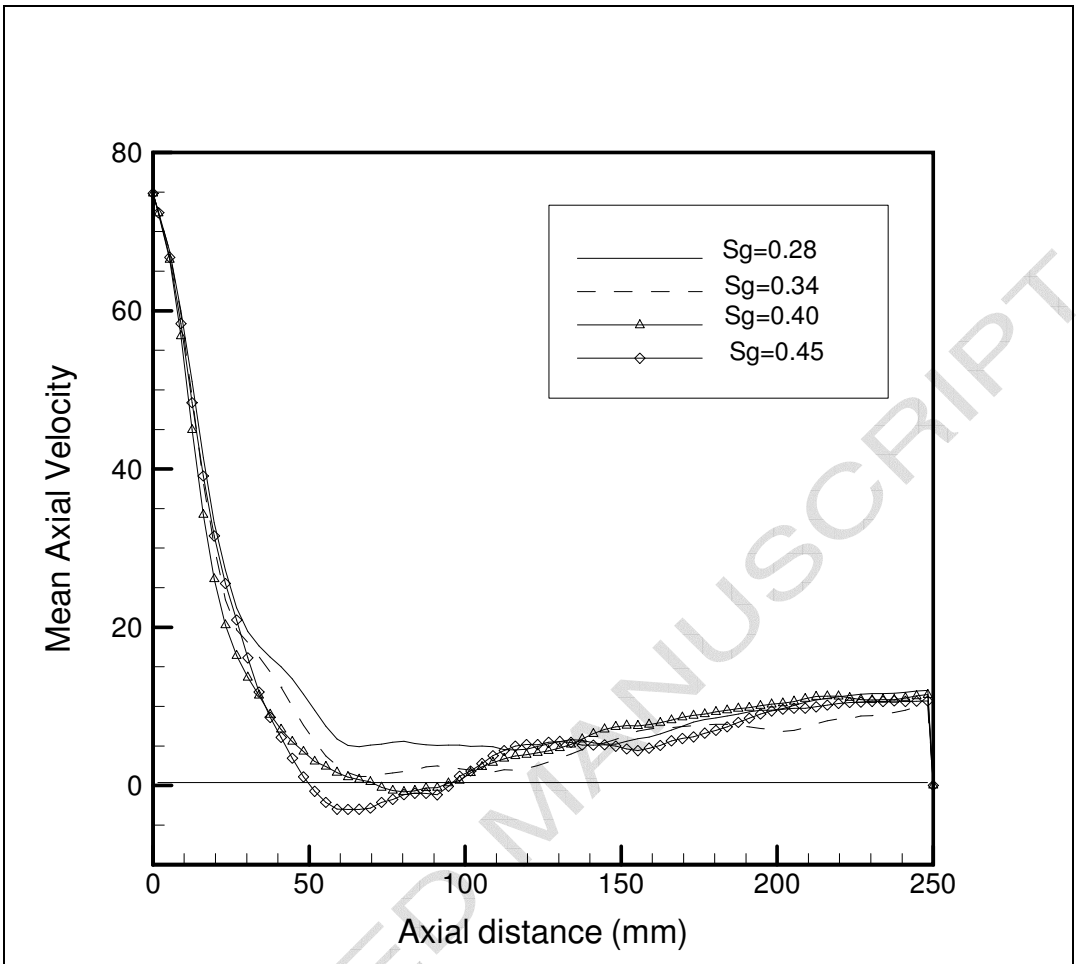

Fig.5. Mean centerline axial velocity for range of swirl numbers at $U_s = 29.7$ m/s

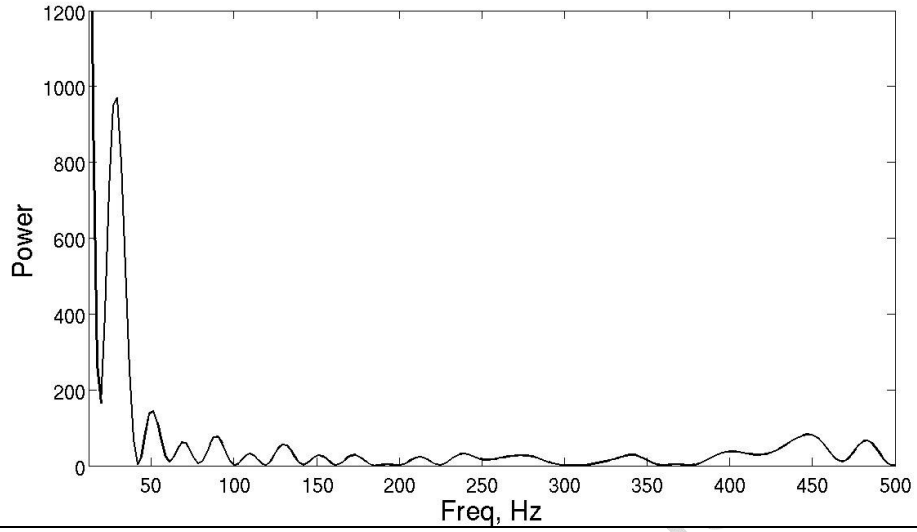

Fig.6. Power spectrum (W/Hz) at spatial jet locator for swirl number 0.34

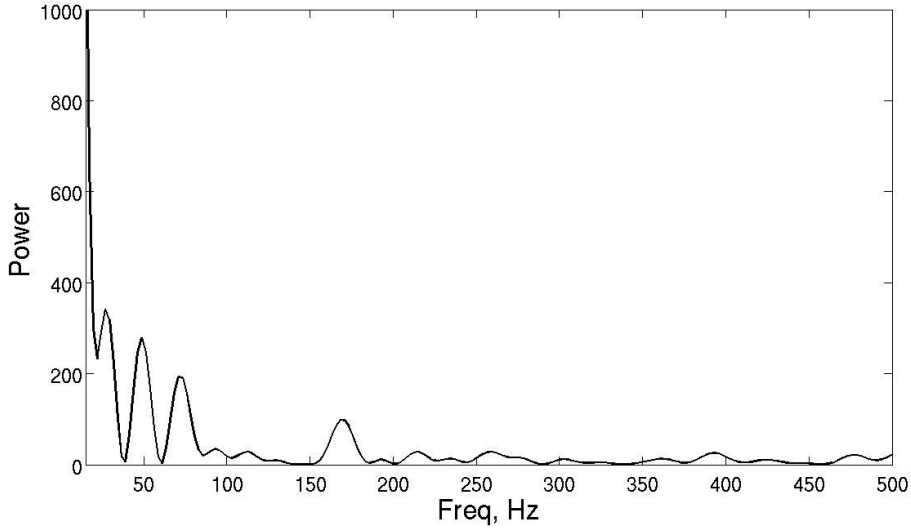

Fig.7. Power spectrum (W/Hz) at spatial jet locator for swirl number 0.40

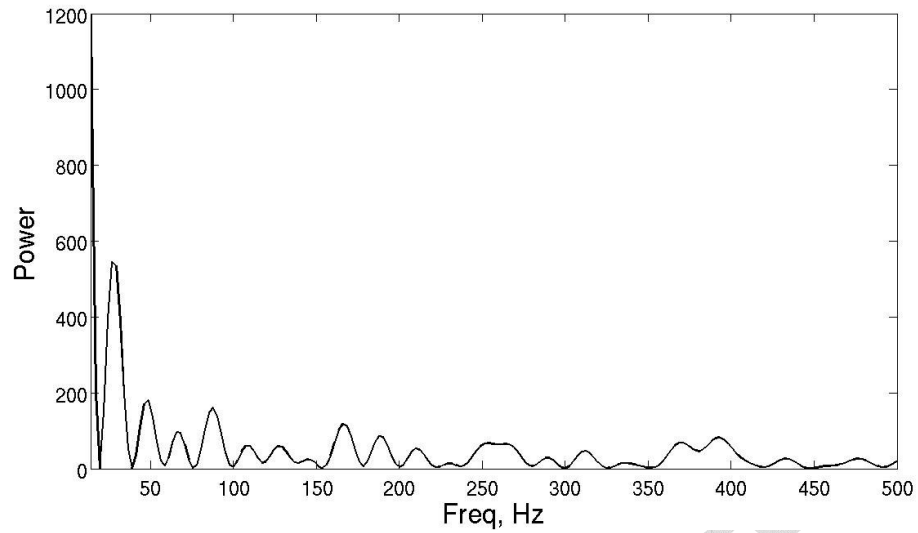

Fig. 8. Power spectrum (W/Hz) at spatial jet locator for swirl number 0.45

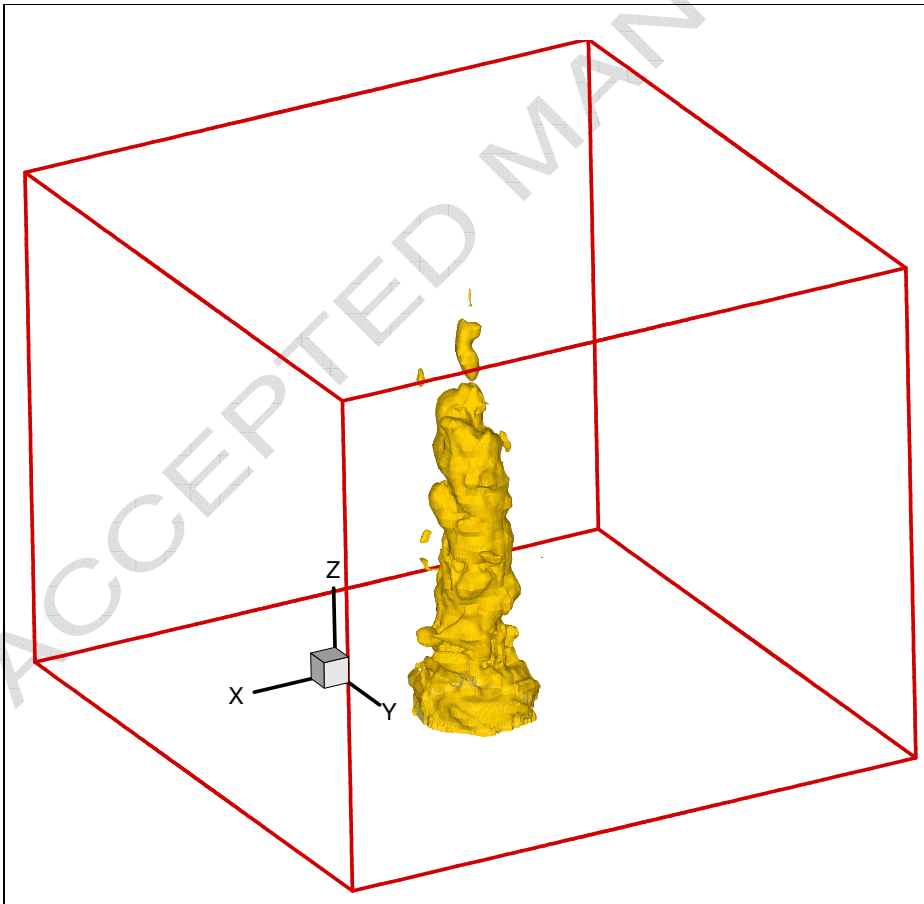

Fig. 9. Precessing vortex core visualised by isocontours of pressure for swirl number 0.40

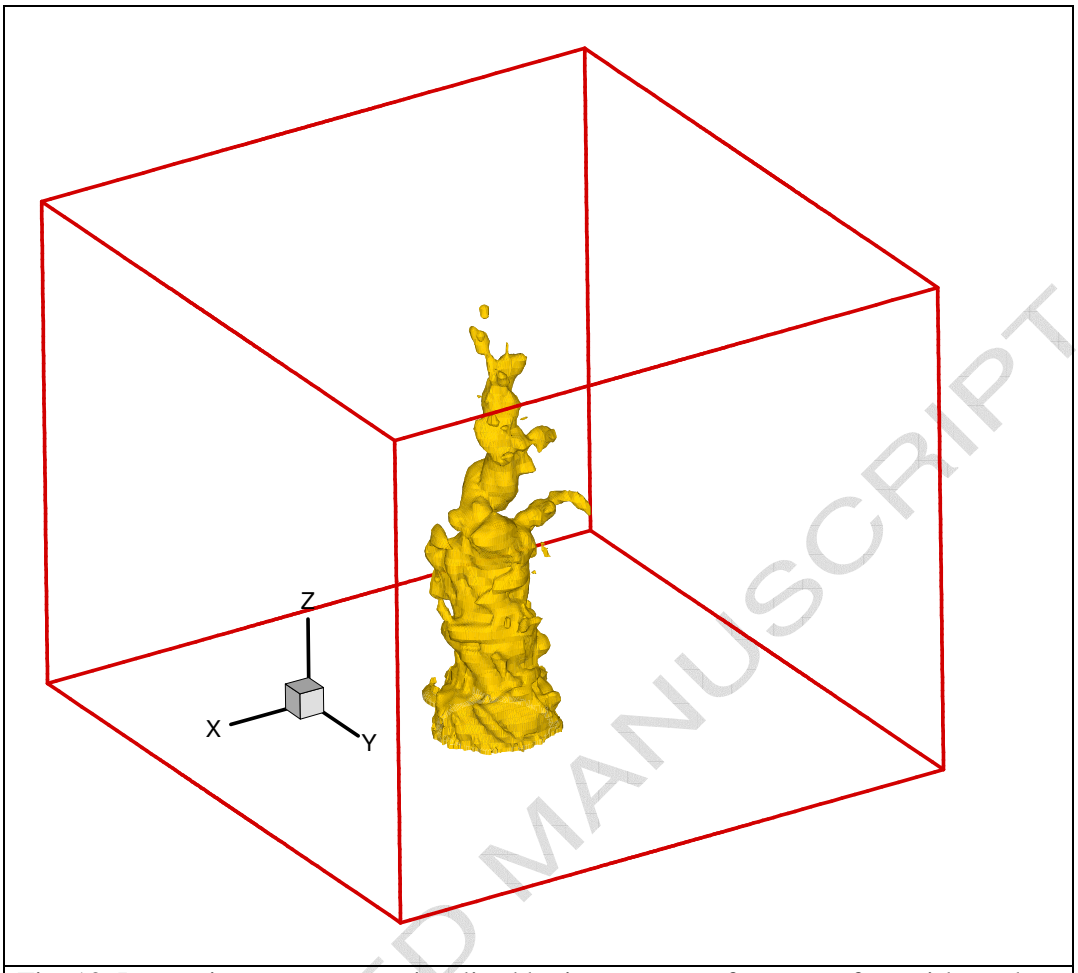

Fig. 10. Precessing vortex core visualised by isocontours of pressure for swirl number 0.45

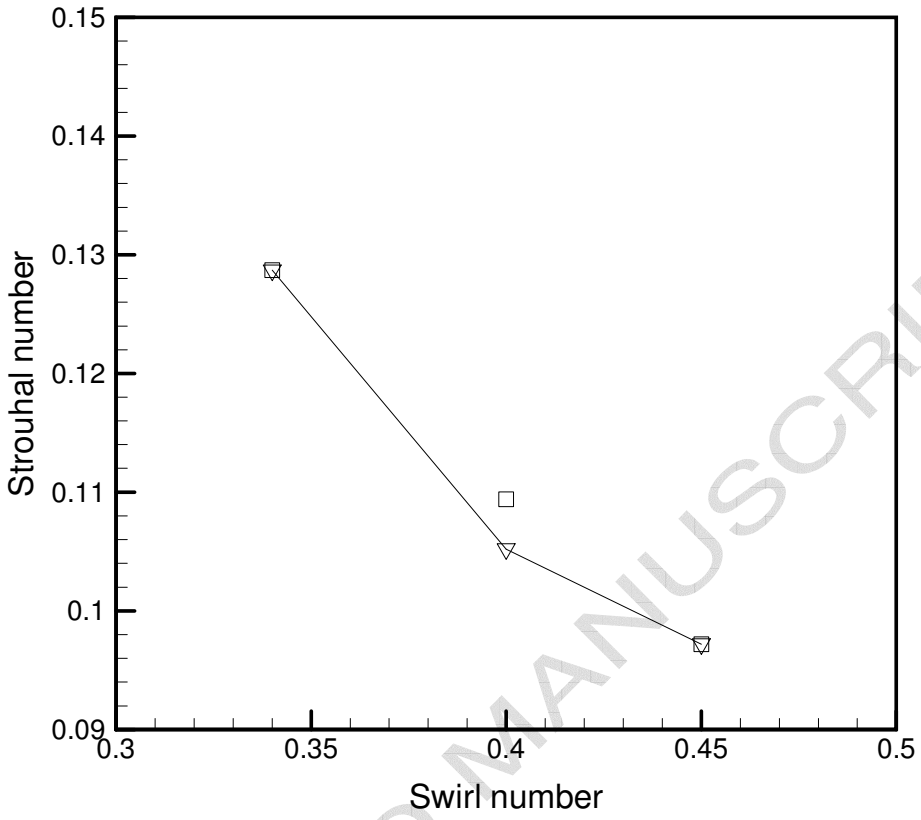

Fig. 11. Variation of Strouhal number with swirl number. Diamonds represent LES results and square symbol represent experimental measurements

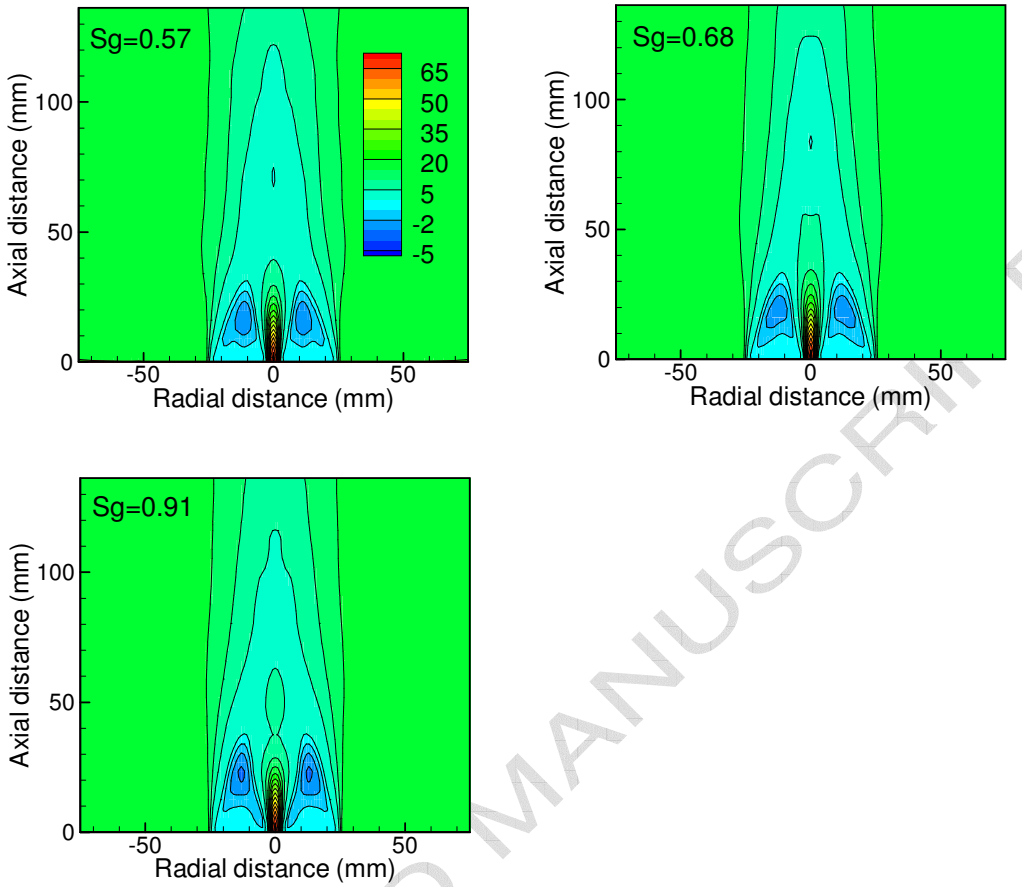

Fig. 12. Contour plots of mean axial velocities (in m/s) at $U_s = 16.3$ m/s

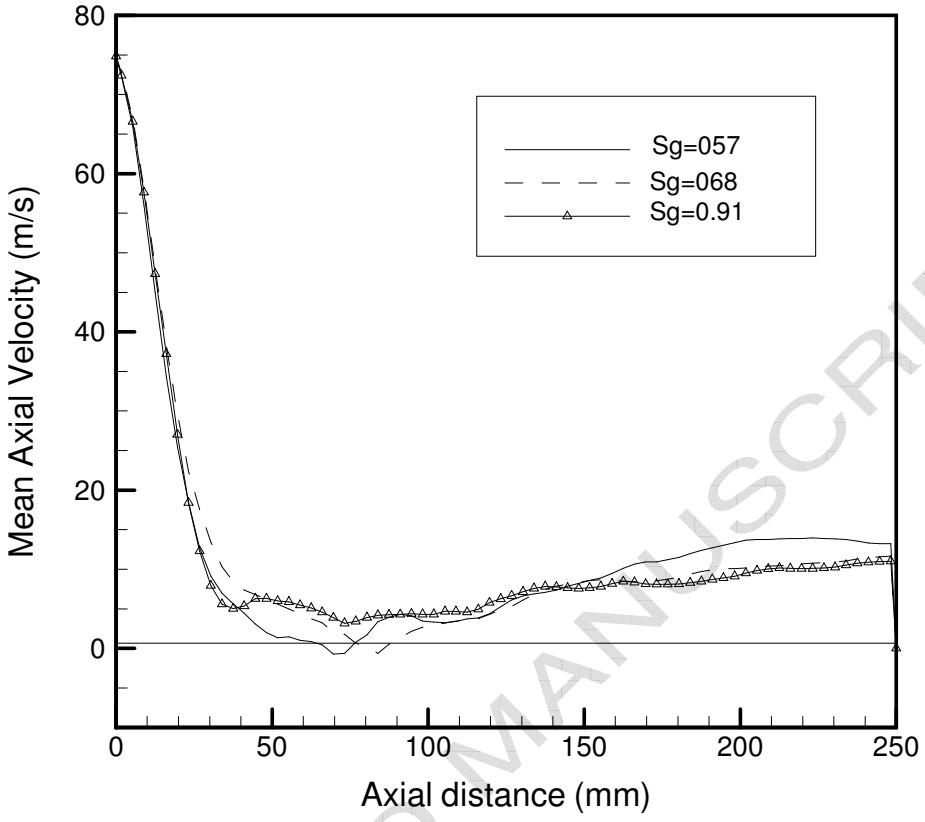

Fig.13. Mean centerline axial velocity for range of swirl numbers at $U_s = 16.3$ m/s

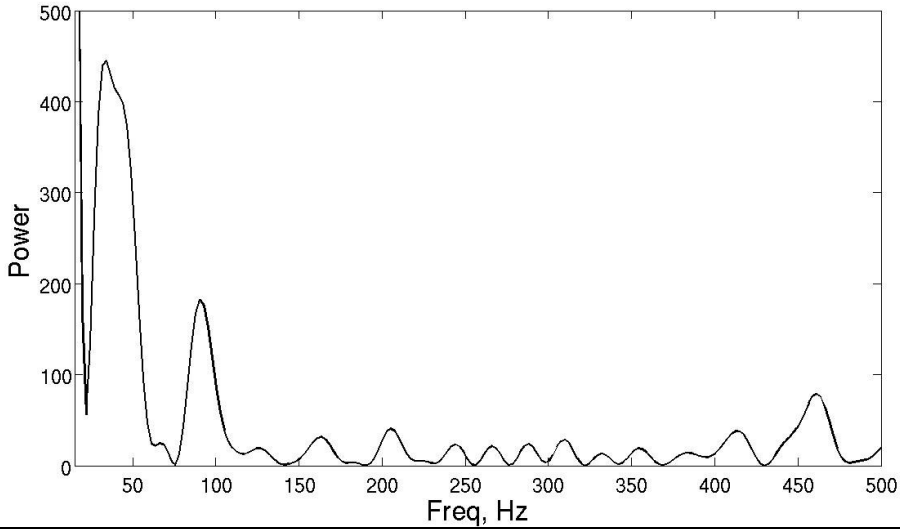

Fig.14. Power spectrum (W/Hz) at spatial jet locator for swirl number 0.57

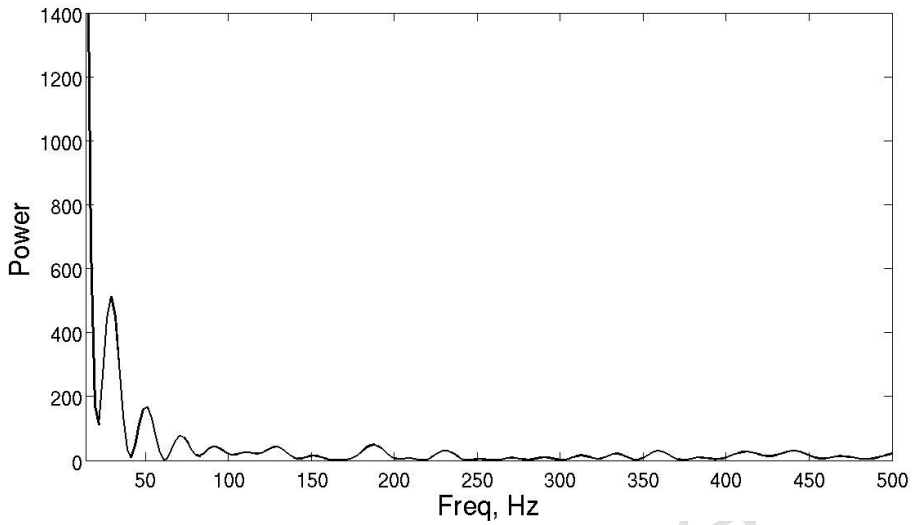

Fig.15. Power spectrum (W/Hz) at spatial jet locator for swirl number 0.68

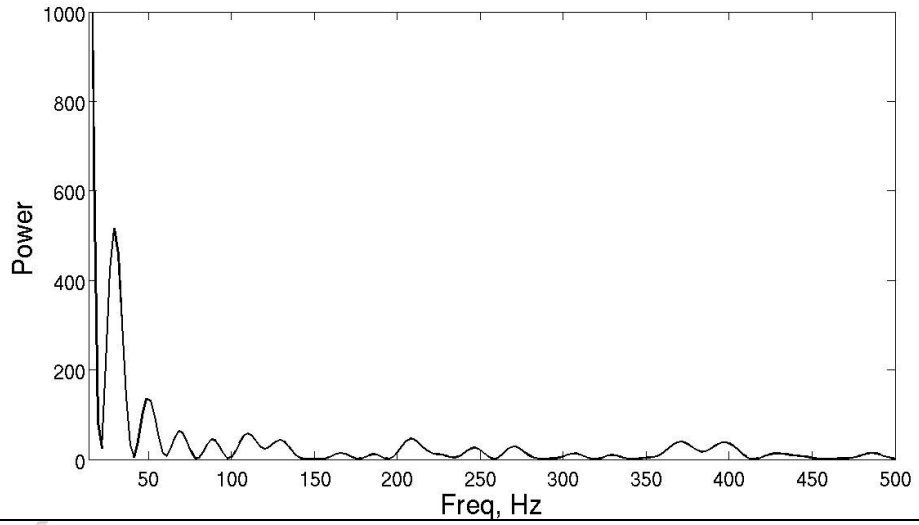

Fig.16. Power spectrum (W/Hz) at spatial jet locator for swirl number 0.91

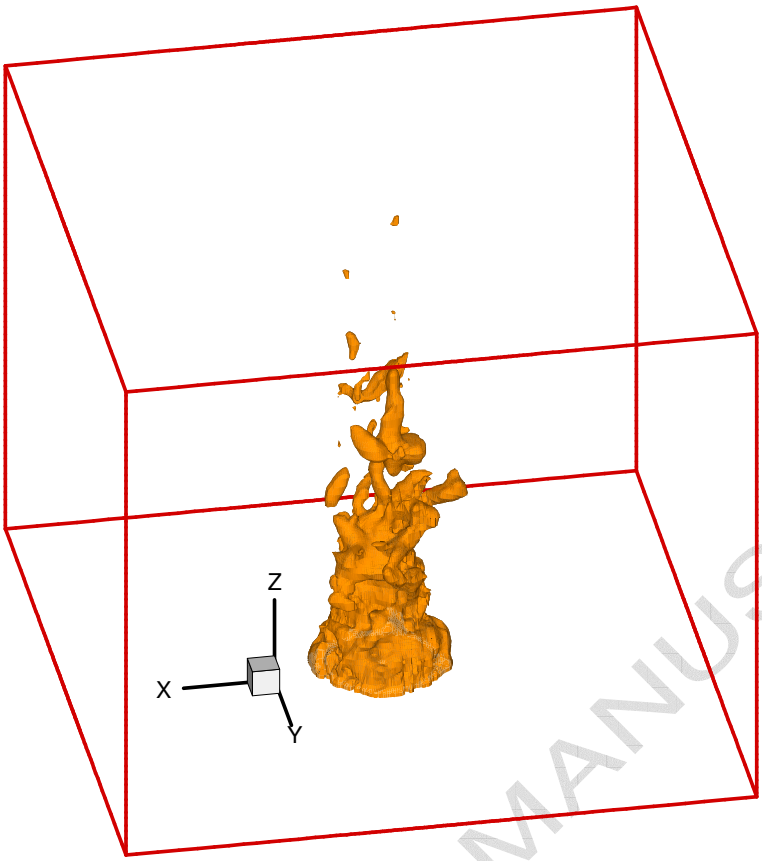

Fig. 17. Precessing vortex core visualised by isocontours of pressure for swirl number 0.57

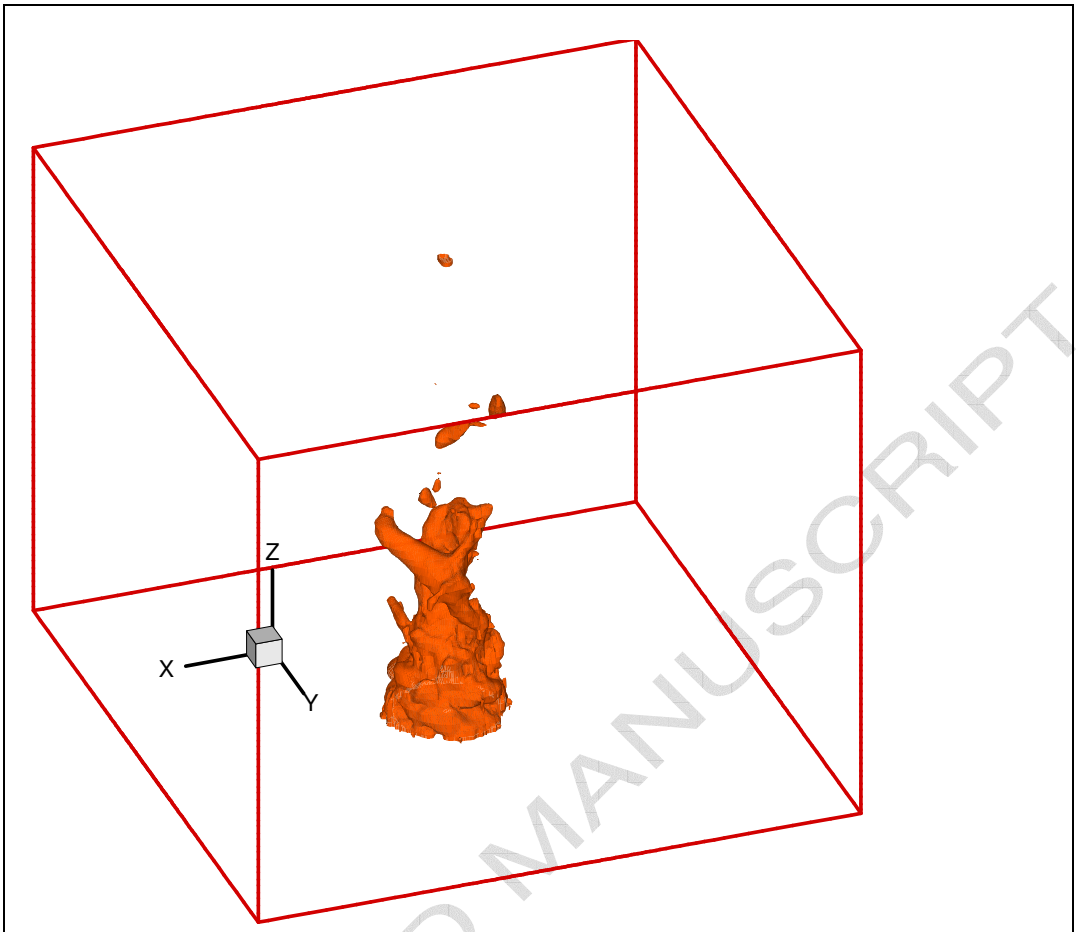

Fig. 18. Precessing vortex core visualised by isocontours of pressure for swirl number 0.68

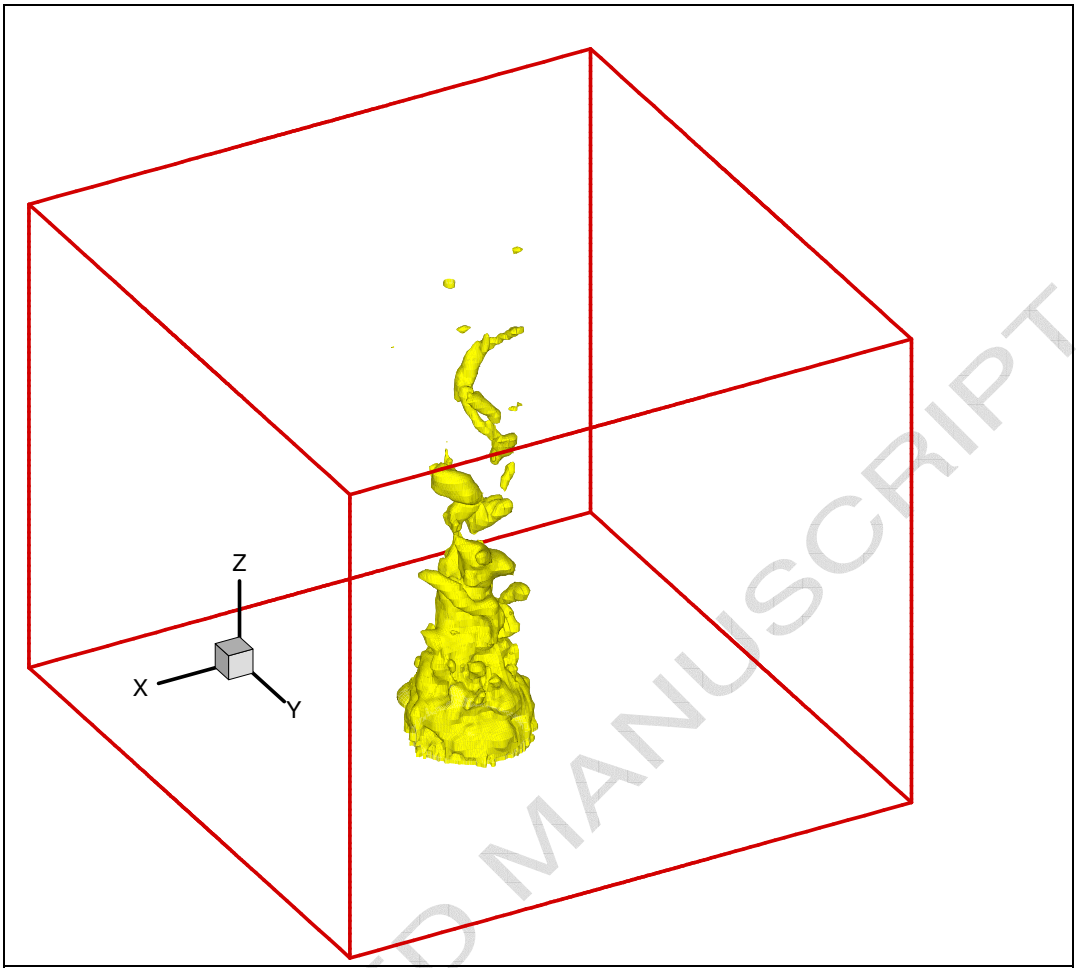

Fig. 19. Precessing vortex core visualised by isocontours of pressure for swirl number 0.91

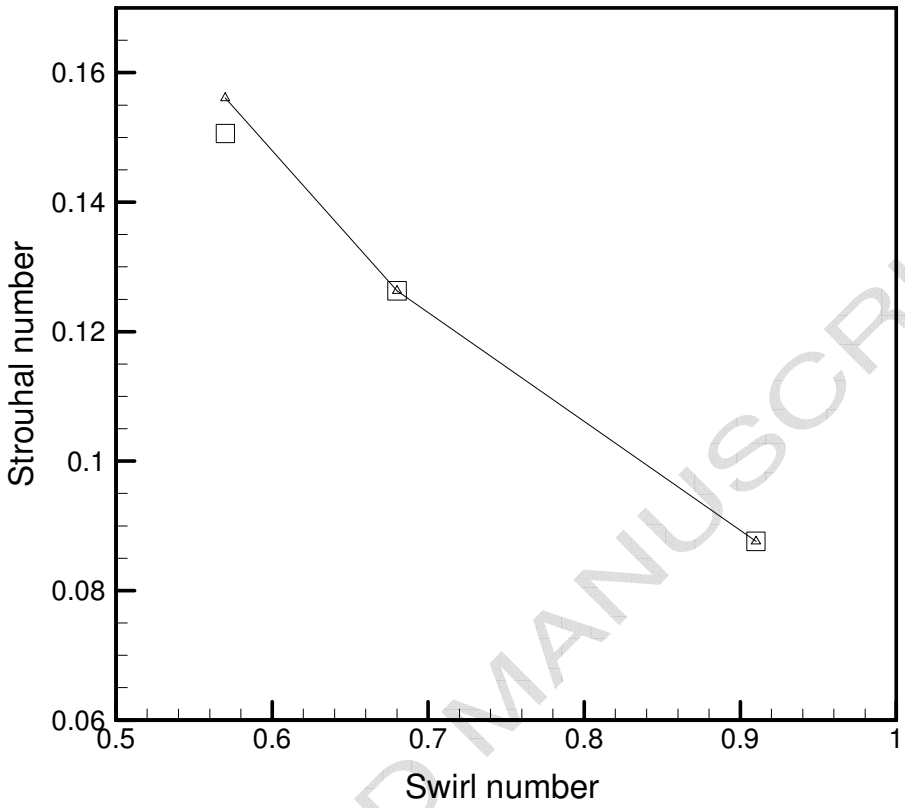

Fig. 20. Variation of Strouhal number with swirl number. Diamonds represent LES results and square symbol represent experimental measurements